Modeling and numerical simulation of action potential patterns in human atrial tissues

Luca Gerardo-Giorda

Modeling and numerical simulation of action potentials in human atrial tissues

Luca Gerardo-Giorda *

Abstract

Electrophysiology of the heart is the subject of a vast interdisciplinary literature, from medical sciences through bio-engineering, physiology, chemistry and physics. The difficulty in having access to direct measures on real patients entailed the coupling of such studies with numerical simulations. Several works have been done on this topic, focusing mainly on the behavior of the ventricles. In this paper we focus on atrial simulation: we present a reaction-diffusion model coupled with the simple FitzHugh-Nagumo (FHN) model and the more complex Courtemanche-Ramirez-Nattel (CRN) model, which has been derived explicitely for human atrial cells. Numerical experiments are performed with both the bidomain and the monodomain models to simulate the evolution of a complete heartbeat.

1 Introduction

The basic property of neural cells to produce signals is called Action Potential (AP). It consists of a sudden variation in the transmembrane potential, called upstroke, followed by a recovering of the resting condition. It shows different shapes and amplitudes according to the different kind of excitable media to which the cells belong to, and in the large muscle cells makes it possible the simultaneous contraction of the whole cell. An action potential propagates keeping the same shape and amplitude all along an entire neural or muscular fiber. Cardiac cells are characterized by a transmembrane potential that is negative at rest, owing to the fact that the concentration of potassium ions $[K^+]_i$ inside the cardiac cell is remarkably higher than the outside concentration $[K^+]_e$, and show two kinds of action potentials: the quick and the slow response.
The quick response is typical in the myocardium fibers (both atrial and ventricular) and in the Purkinje fibers, which are fibers specialized in the conduction. The quick response cells are characterized by a negative transmembrane potential at rest (around -90mV), and by a rapid depolarization (positive overshoot), where the potential difference changes sign and the internal potential overtakes the external one of around 20mV: such phase is called Phase 0. Immediately after that (Phase 1) a short period of partial repolarization takes place, followed by a plateau (Phase 2) which lasts for around 0.2 seconds. The potential gets progressively more negative (Phase 3) until it reaches again the resting value. The repolarization procedure is far slower than the depolarization one, and the interval between the end of the repolarization and the next action potential is called Phase 4.
The slow response is the one taking place in the Sinoatrial Nodus (SA), the natural pacemaker of the heart, and in the Atrioventricular Nodus (AV), the tissue meant to transfer the pulse from atria to ventricles. The slow response cells are characterized by a resting potential less negative (around -50mV), by a smaller slope and amplitude in the overshoot of the action potential, by the absence of the Phase 1, and by a relative refractory period that continues during Phase 4.
The Action Potential propagates across the heart in an heterogeneous way. The pulse moves from the Sinoatrial Nodus (SA), and propagates through the ordinary myocardic fibers of the right atrium, while the Buchmann's bundle drives the pulse towards the left atrium. Some action potentials propagate downwards and reach the Atrioventricular Nodus (AV), which is, under normal conditions, the only gate for the pulse

*Department of Mathematics and Computer Science, Emory University, 400 Dowman Drive, 30322 Atlanta, USA - email: luca@mathcs.emory.edu

to propagate from atria to ventricles, where the conduction is quicker ($4\ ms^{-1}$ versus $1\ ms^{-1}$).
The electrical activity of the heart as a whole is thus characterized by a complex multiscale structure, ranging from the microscopic activity of ion channels in the cellular membrane to the macroscopic properties of the anisotropic propagation of the excitation and recovery fronts in the whole heart. The most complete model of such a complex setting is the anisotropic Bidomain model (see [9, 25]), that consists of a system of two degenerate parabolic reaction-diffusion equations describing the intra and extracellular potentials in the cardiac muscle, coupled with a system of ordinary differential equations describing the ionic currents flowing through the cellular membrane, that are associated to the nonlinear reaction term. This model is computationally very expensive because of the involvement of different space and time scales, and a simplified tissue model is the anisotropic Monodomain system, consisting of a parabolic reaction-diffusion equation describing the propagation of the transmembrane potential coupled with an ionic model, which has been widely used in literature (see for instance [23, 19]).
If, on the one hand, a wide literature is available for ventricular models (see for instance [4, 5, 20] and references therein), on the other hand less has been done on atria, although Atrial Fibrillation (AF) is the most commonly sustained arrhythmia, for which clinical treatment remains the most problematic. Knowledge of the human atrial Action Potential and of its ionic currents is thus of critical importance to understand the electrical properties of atrial tissues in both normal and pathological conditions.
In this paper we consider the FitzHugh-Nagumo (FHN) cell model in the Rogers-McCulloch variant, which is well suited to capture the excitation wavefront, but behaves very poorly in the description of the plateau phase, and the Courtemanche-Ramirez-Nattel (CRN) model, that is especially designed for human atrial myocytes. Both models are then coupled with monodomain and bidomain simulations on a two dimensional slab with anisotropic conduction.
The rest of the paper is organized as follows. In Section 2 we give a brief review of the mathematical models, the anisotropic bidomain and monodomain ones. In Section 3 we describe the ionic currents and the modified FHN and the CRN membrane models. In Section 4 we formulate the finite dimensional approximation of the problem. Finally, in Section 5, some numerical simulations are presented, varying both the cardiac tissue model (monodomain and bidomain) and the ionic model (FHN and CRN).

2 Description of the model

The conductivity of the cardiac cells depends upon their orientation, and in the most general case the conductivity tensor is anisotropic. The structure of the cardiac cells can be modeled, following Le Grice *et al.* ([15]) as a sequence of muscular layers going from endocardium to epicardium (see also [29]). In any point $\mathbf{x} \in \Omega$ (in the rest of the paper Ω will denote the spatial domain under consideration) it is thus possible to identify an orthonormal triplet of directions, $\mathbf{a}_l(\mathbf{x})$, $\mathbf{a}_t(\mathbf{x})$, $\mathbf{a}_n(\mathbf{x})$, with $\mathbf{a}_l(\mathbf{x})$ parallel to the fibers direction, $\mathbf{a}_t(\mathbf{x})$ and $\mathbf{a}_n(\mathbf{x})$ tangent and orthogonal repectively to the radial lamination, both transversal with respect to the fiber axis.
The bidomain model consists in representing the cardiac tissue as the superposition of two media which are continuous and anisotropic, the intra-cellular and the extra-cellular one, coexisting at each point $\mathbf{x}$ and separated by a cell membrane. Such model has been derived, by an homogenization technique, starting from a periodic assembling of elongated cells surrounded by extracellular space and connected by end-to-end or side-to-side junctions (for the mathematical details we refer to [13, 6]).
Denoting by $\sigma_l^{i,e}$, $\sigma_t^{i,e}$, and $\sigma_n^{i,e}$ the conductivity coefficients in the $\mathbf{a}_l$, $\mathbf{a}_t$ and $\mathbf{a}_n$ directions, the conductivity tensor is given by

$$D_{i,e}(\mathbf{x}) = \sigma_l^{i,e}\mathbf{a}_l(\mathbf{x})\mathbf{a}_l^T(\mathbf{x}) + \sigma_t^{i,e}\mathbf{a}_t(\mathbf{x})\mathbf{a}_t^T(\mathbf{x}) + \sigma_n^{i,e}\mathbf{a}_n(\mathbf{x})\mathbf{a}_n^T(\mathbf{x}),$$

for the intra- and extra-cellular medium respectively.
The intra-cellular and extra-cellular electric potentials, which we denote by u_i and u_e, are governed in the bidomain model by a degenerate reaction diffusion system of parabolic type, coupled with an ODE system describing the ionic gating variables w and the ionic concentrations c. In the following we denote by $v = u_i - u_e$ the transmembrane potential. The membrane current per unit volume is given by

$$I_m = c_m\partial_t v + I_{ion}(v, w, c), \tag{2.1}$$

where $c_m = \chi C_m$, $I_{ion} = \chi i_{ion}$, χ being the membrane area per tissue volume, C_m the surface capacity and i_{ion} the membrane ionic current per unit area.
We assume that any external current can be applied to the extracellular medium only: such current, that we denote by I_e^{app}, has to satisfy a zero mean value compatibility condition $\int_\Omega I_e^{app} = 0$. Denoting by $\mathbf{J}_i = -D_i \nabla u_i$ and $\mathbf{J}_e = -D_e \nabla u_e$ the intracellular and extracellular current densities, respectively, the bidomain model is derived by imposing the conservation of the total current and in given by

$$\operatorname{div} \mathbf{J}_i = -I_m \qquad \operatorname{div} \mathbf{J}_e = I_m - I_e^{app} \tag{2.2}$$

The ionic current through membrane channels in (2.1) depends on the transmembrane potential v, on M_w gating variables $w \in \mathbb{R}^{M_w}$, and on M_c concentration variables $c \in \mathbb{R}^{M_c}$ and, in an Hodgkin-Huxley formalism, reads

$$I_{ion}(v, w, c) = \sum_{l=1}^{L} G_l(v) \Phi_l(c) \prod_{j=1}^{M_w} w_j^{p_{jl}} (v - v_l(w)),$$

$G_k(v)$ being the membrane conductance, v_k being the reversal potential for the k-th current, p_{jk} being integers, $\Phi_l(c)$ is a (possibly) nonlinear function of the concentrations, and where the dynamics of the gating and concentration variables is described by a system of ODE's

$$\frac{\partial w}{\partial t} = R(v, w) \qquad \frac{\partial c}{\partial t} = S(v, w, c), \tag{2.3}$$

with prescribed initial condition $w(\mathbf{x}, 0) = w_0(\mathbf{x})$ and $c(\mathbf{x}, 0) = c_0(\mathbf{x})$. In such models, for any gating variable w_j, we have $0 < w_j < 1$, and the right hand side $R_j(v, w)$ has a special structure such that the system is decoupled and the corresponding ODE is given by

$$\frac{\partial w_j}{\partial t} = R_j(v, w) = R_j(v, w_j) = \alpha_j(v)(1 - w_j) - \beta_j(v) w_j, \tag{2.4}$$

with $\alpha_j(v), \beta_j(v) > 0$.
Owing to (2.1) and (2.2), the bidomain model in the variables $(u_i(\mathbf{x}, t), u_e(\mathbf{x}, t))$ and $v(\mathbf{x}, t) = u_i(\mathbf{x}, t) - u_e(\mathbf{x}, t)$, for an insulated domain $\Omega \subset \mathbb{R}^3$, eventually reads

$$\begin{cases} c_m \partial_t v - \operatorname{div}(D_i \nabla u_i) + I_{ion}(v, w, c) = 0 & \text{in } \Omega \times (0, T) \\ -c_m \partial_t v - \operatorname{div}(D_e \nabla u_e) - I_{ion}(v, w, c) = -I_e^{app} & \text{in } \Omega \times (0, T) \\ \partial_t w - R(v, w) = 0 & \text{in } \Omega \times (0, T) \\ \partial_t c - S(v, w, c) = 0 & \text{in } \Omega \times (0, T) \\ \mathbf{n}^T D_{i,e} \nabla u_{i,e} = 0 & \text{in } \partial\Omega \times (0, T) \\ v(\mathbf{x}, 0) = v_0(\mathbf{x}) \qquad w(\mathbf{x}, 0) = w_0(\mathbf{x}) \qquad c(\mathbf{x}, 0) = c_0(\mathbf{x}) & \text{in } \Omega. \end{cases} \tag{2.5}$$

The above system uniquely determines v, whereas the potentials u_i and u_e are determined modulus an additive constant depending on time and linked to the reference potential. Such potential is chosen as the mean extracellular potential in the cardiac volume, by imposing a zero mean condition $\int_\Omega u_e = 0$.
System (2.5) can be rewritten in terms of the extracellular and the transmembrane potentials. From the second equation in (2.5) we get

$$c_m \partial_t v = -\operatorname{div}(D_e \nabla u_e) - I_{ion}(v, w, c) - I_e^{app},$$

and inserting it into the first one provides

$$-\operatorname{div}\ [D_i \nabla u_i + D_e \nabla u_e] = -I_e^{app}.$$

So far, adding and subtracting $\operatorname{div}(D_i \nabla u_e)$, we obtain the formulation in terms of v and u_e:

$$\begin{cases} -c_m \partial_t v - \operatorname{div}(D_e \nabla u_e) - I_{ion}(v, w, c) = -I_e^{app} & \text{in } \Omega \times (0, T) \\ -\operatorname{div}\ [(D_i + D_e) \nabla u_e] = \operatorname{div}(D_i \nabla v) - I_e^{app} & \text{in } \Omega \times (0, T) \end{cases} \tag{2.6}$$

If we assume the anisotropy ratio to be the same in the two media, intra- and extra-cellular, namely we assume $D_i = \lambda D_e$ with λ constant, the bidomain model reduces to a simpler one. If we let

$$D = \frac{\lambda}{1+\lambda} D_i, \qquad I^{app} = \frac{\lambda}{1+\lambda} I_i^{app} + \frac{1}{1+\lambda} I_e^{app},$$

the simplified model consists of a single reaction-diffusion equation of parabolic type for the transmembrane potential v,

$$c_m \partial_t v - \operatorname{div}(D(\mathbf{x})\nabla v) + I_{ion}(v, w, c) = I^{app} \qquad \text{in } \Omega \times (0, T), \tag{2.7}$$

coupled with the ODE system (2.3) for the gating and concentration variables. Such model is referred to as monodomain model.

3 Ionic currents and membrane models

The ionic currents appearing in both the monodomain and the bidomain model rely on the choice of the membrane model for the cell conductivity. The earliest model appeared in the work on nerve action potential by Hodgkin and Huxley ([10]), which earned them the Nobel prize in Medicine in 1963. Models of this type have then been extensively studied and developed by physiologists for the cardiac action potential: under the assumption of an equipotential cell, the variation in time of the membrane potential v for a single cells is ruled in such models by an ordinary differential equation

$$\frac{dv}{dt} = -\frac{I_{ion} - I_{st}}{C_m}, \tag{3.1}$$

where I_{ion} and I_{st} are the total ionic current and stimulus current across the membrane, respectively, and C_m is the total membrane capacitance. Such models are naturally included in the above framework, where the stimulus current is provided by the diffusive term in both the bidomain and the monodomain settings, modeling the stimulus propagation through neighboring cells.

Concerning the modeling of ventricular cells, the fitting of improved experimental data with more complex models led to the developement of many refinements of the original Hodgkin-Huxley model: among them, we recall the model by Beeler and Reuter (1977, with 4 ionic currents and 7 gating and concentrations variables), and the phase-I Luo-Rudy (1991, with $N = 6$ and $M = 7$). In this direction, the most recent published model of mammalian ventricular cells is the phase-II Luo-Rudy (1994, [17]), which is based on measurements from guinea pig. Simpler models of reduced complexity have also been proposed, where only 1 or 2 gating variables are considered.

If, on the one hand, several models are available to describe the behaviour of ventricular cells, less has been done focusing on atrial cells. Atria differ from ventricles under several aspects. First of all, the thickness of the wall in atria is far less significant than in ventricles, while the speed of conduction is much larger in ventricles. A different ionic current and membrane model should therefore be used when dealing with atria. In this direction, models of atrial cells based on animal data only have been published (see [8, 22, 31]): the most recent of such models is the one proposed by Lindblad *et al.* (1996, [16]), which is based on measurements from rabbit atrial cells. Although these models have provided valuable insights into the mechanisms underlying the action potential generation in animals, the significant interspecies differences with respect to human being and the amount of available human data led scientists to develop mathematical models of the action potential based on ionic current data measured directly in human atrial cells. The most recently published models in this direction are the ones proposed by Nygren *et al.* in [18] and by Courtemanche *et al.* in [7]. Both models handle the atrial cell as a capacitor connected in parallel with variable resistances and batteries representing the ionic channels and driving forces.

3.1 The FHN cell model

The simplest ionic model is the FitzHugh-Nagumo (FHN), consisting of 1 ionic current and 1 gating variable. Assuming the potential v to be zero at rest, the ionic current uses only one recovery variable:

$$I_{ion}(v, w) = g(v) + \beta w,$$

where $\beta > 0$, $g(v)$ is a cubic-like function, and w satisfies

$$\frac{\partial w}{\partial t} = \eta v - \gamma w,$$

with $\eta, \gamma > 0$. Such model is well suited to represent neural cells, but this is not the case for the physiological description of cardiac cells: in particular, the overshoot phase lacks in sharpness and during the recovering phase the potential falls below the resting value.
An improvement of this model is given by the following variant by Rogers and McCulloch ([23]):

$$I_{ion}(v, w) = Gv\left(1 - \frac{v}{v_{\text{th}}}\right)\left(1 - \frac{v}{v_{\text{p}}}\right) + \eta_1 v w,$$

$$\frac{\partial w}{\partial t} = \eta_2\left(\frac{v}{v_{\text{p}}} - \eta_3 w\right),$$

where $G, \eta_1, \eta_2, \eta_3$ are positive coefficients, v_{th} is a threshold potential, and v_{p} is the peak potential. In Figure 1 we report the time evolution of the potential v and of the gating variable w for the Rogers-McCulloch variant of the FHN model.
The great simplicity of this model is behind its wide use in literature. However, if on the one hand, such model is well suited to describe the positive overshoot in the quick depolarization phase, on the other hand it provides only a coarse approximation in the plateau and repolarization phases of the action potential, and behaves too poorly when accuracy in the description of the action potential is needed.

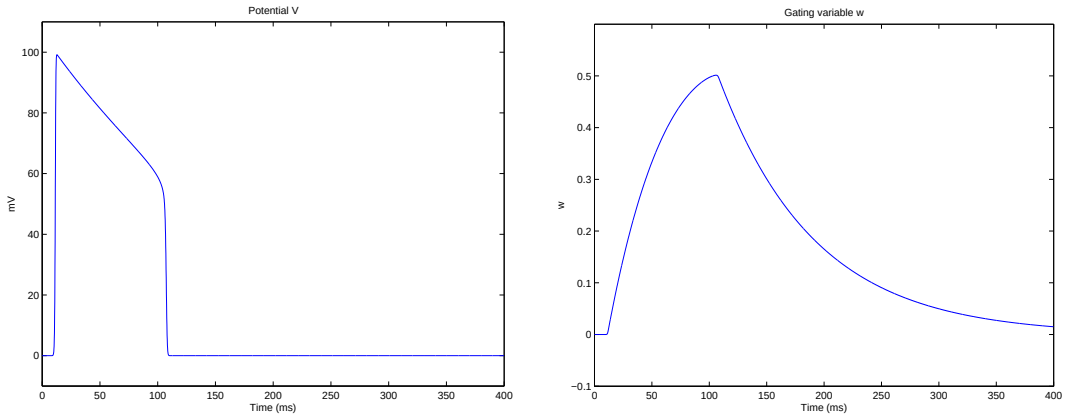

Figure 1: Time evolution of the potential v and the gating variable w in the Rogers-McCulloch variant of the FHN model

3.2 The CRN atrial cell model

One of the most accurate models for atrial cells is the CRN (Courtemanche, Ramirez and Nattel, [7]) one, in which the total ionic current is given by the sum

$$I_{\text{ion}} = I_{\text{Na}} + I_{\text{K}} + I_{\text{Ca}} + I_{\text{b}} + I_{\text{p}}. \tag{3.2}$$

The above expression takes into account several aspects of the action potential generation. In (3.2), I_{Na} is the fast depolarizing Na^+ current, while the quantity I_{K} is the total rectifier K^+ current, given by

$$I_{\text{K}} = I_{\text{K1}} + I_{\text{to}} + I_{\text{Kur}} + I_{\text{Kr}} + I_{\text{Ks}},$$

where I_{K1} is the inward rectifier K^+ current, playing a major role in the late repolarization phase of the AP and in determining resting membrane potential and resistance, I_{to} is the transient outward K^+ current,

I_{Kur}, I_{Kr}, and I_{Ks} are the ultrarapid, rapid, and slow rectifier currents. The quantity $I_{\mathrm{Ca}} = I_{\mathrm{Ca,L}}$ is the L-type Ca^{2+} current, while I_{b} is the the background current for sodium Na^{+} and calcium Ca^{2+}

$$I_{\mathrm{b}} = I_{\mathrm{b,Na}} + I_{\mathrm{b,Ca}}.$$

Finally, I_{p} collects the actions of pumps and ion exchangers, designed to put back into balance the ion concentrations at rest:

$$I_{\mathrm{p}} = I_{\mathrm{NaCa}} + I_{\mathrm{NaK}} + I_{\mathrm{p,Ca}},$$

where I_{NaCa} is the sodium-calcium pump, I_{NaK} is the sodium-potassium pump, and $I_{\mathrm{p,Ca}}$ is the calcium exchanger.

The model handles also the intracellular concentrations $[Na^{+}]_i$, $[K^{+}]_i$, and $[Ca^{2+}]_i$, as well as the intracellular calcium buffering by the sarcoplasmic reticulum system (SR), by means of the calcium concentrations in the uptake ($[Ca^{2+}]_{\mathrm{up}}$), and release ($[Ca^{2+}]_{\mathrm{rel}}$) SR compartments.

In the model, no extracellular cleft space is included, the membrane capacitance is $c_m = 100\mathrm{pF}$, the lenght and diameter of the cells are set to 100 and 16 μm, respectively, and the cell compartment volumes are the same ones used in the phase-II Luo-Rudy model (LR2, [17]). Denoting by E_X the equilibrium potential for ion X, and with g_X its maximal conductance, from Nerst equation, E_X is given by

$$E_X = \frac{RT}{zF} \log \frac{[X]_e}{[X]_i},$$

where R is the gas constant, T is the absolute temperature, F is the Faraday constant, $z = 1$ for Na^{+} and K^{+}, $z = 2$ for Ca^{2+}, and $[X]_e$ and $[X]_i$ denote the external and internal concentration of ion X.

The ionic currents are all voltage-dependent, and, in addition, some of them depend upon gating variables whose activation or deactivation handles the ions passage across the membrane, according to the phase of the action potential. The generic gating variable y satisfies an ordinary differential equation such

$$\frac{dy}{dt} = -\frac{y^{\infty} - y}{\tau_y}, \tag{3.3}$$

where y^{∞} is the steady state of the gating variable with the cell at rest. Notice that formulation (3.3) falls into the Hodgkin-Huxley formalism by setting

$$y^{\infty} = \alpha_y(v)\tau_y(v) \qquad\qquad \tau_y(v) = \frac{1}{\alpha_y(v) + \beta_y(v)}.$$

The dynamics of the concentration variables is governed by the following equations

$$\frac{d[Na^{+}]_i}{dt} = \frac{-3I_{\mathrm{NaK}} - 3I_{\mathrm{NaCa}} - I_{\mathrm{b,Na}} - I_{\mathrm{Na}}}{FV_i} \tag{3.4}$$

$$\frac{d[K^{+}]_i}{dt} = \frac{2I_{\mathrm{NaK}} - I_{\mathrm{K1}} - I_{\mathrm{to}} - I_{\mathrm{Kur}} - I_{\mathrm{Kr}} - I_{\mathrm{Ks}}}{FV_i} \tag{3.5}$$

$$\begin{aligned}\frac{d[Ca^{2+}]_i}{dt} = &\left[\frac{2I_{\mathrm{NaCa}} - I_{\mathrm{p,Ca}} - I_{\mathrm{Ca,L}} - I_{\mathrm{b,Ca}}}{2FV_i} + \frac{V_{\mathrm{up}}(I_{\mathrm{up,leak}} - I_{\mathrm{up}}) + I_{\mathrm{rel}}V_{\mathrm{rel}}}{V_i}\right] \times \\ &\times \left[1 + \frac{\alpha_i\beta_i}{([Ca^{2+}]_i + \beta_i)^2} + \frac{\gamma_i\delta_i}{([Ca^{2+}]_i + \delta_i)^2}\right]^{-1}\end{aligned} \tag{3.6}$$

$$\frac{d[Ca^{2+}]_{\mathrm{up}}}{dt} = I_{\mathrm{up}} - I_{\mathrm{up,leak}} - I_{\mathrm{tr}}\frac{V_{\mathrm{rel}}}{V_{\mathrm{up}}} \tag{3.7}$$

$$\frac{d[Ca^{2+}]_{\mathrm{rel}}}{dt} = (I_{\mathrm{tr}} - I_{\mathrm{rel}})\left[1 + \frac{\alpha_{\mathrm{rel}}\beta_{\mathrm{rel}}}{([Ca^{2+}]_{\mathrm{rel}} + \beta_{\mathrm{rel}})^2}\right]^{-1}, \tag{3.8}$$

where V_i is the intracellular volume, V_{up} and V_{rel} are the volumes of the uptake and release compartments of the sarcoplasmic reticulum (SR), α_i, γ_i, and α_{rel} depend on the total concentrations of troponin and calmodulin in myoplasm, and of calsequestrin in the release compartment of SR, while β_i, δ_i, and β_{rel} depend on their half saturation constants, respectively. All these three proteins are responsible of the

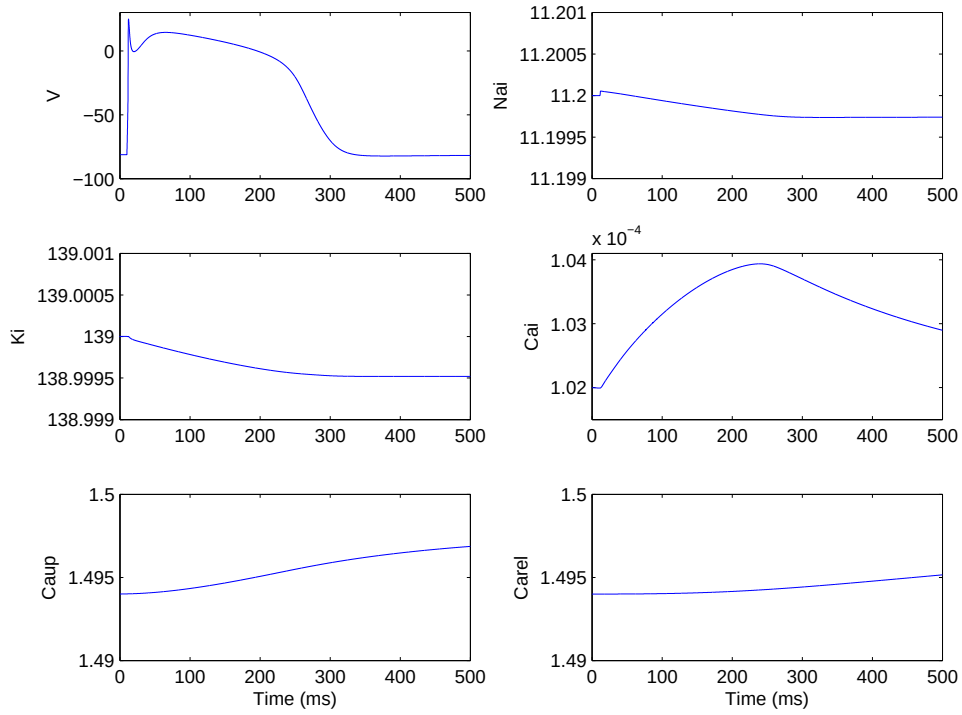

Figure 2: CRN model: potential and concentration variables.

contraction of the cell.
In (3.6) and (3.7), $I_{\text{up,leak}}$ is the Ca^{2+} leak current by the JSR, I_{up} is the Ca^{2+} uptake current by the JSR, while I_{rel} is the Ca^{2+} release current from the JSR. Finally, in (3.7) and (3.8), I_{tr} is the transfer current from NSR to JSR.
The model consists globally of 5 concentration variables and 15 gating variables. In Table 1 we report the gating variables associated to the ionic currents, while in Figure 2 and 3 we plot the time evolution of the potential and of the gating and concentration variables. For a more detailed description of the model we refer the interested reader to the original paper by Courtemanche *et al.* [7].

Current	Gating variables	Current	Gating variables
I_{Na}	$m \quad h \quad j$	I_{Ks}	x_s
I_{to}	$o_a \quad o_i$	$I_{\text{Ca,L}}$	$d \quad f \quad f_{\text{Ca}}$
I_{Kur}	$u_a \quad u_i$	I_{rel}	$u \quad \nu \quad w$
I_{Kr}	x_r		

Table 1: Ionic currents and corresponding gating variables

4 Finite dimensional approximation of the model

In this section we outline the variational formulation of the bidomain and the monodomain models, as well as their finite dimensional approximation. In that order, let $H^1(\Omega)$ be the usual Sobolev space over $\mathbb{R}$. The variational formulation of the bidomain model reads as follows.

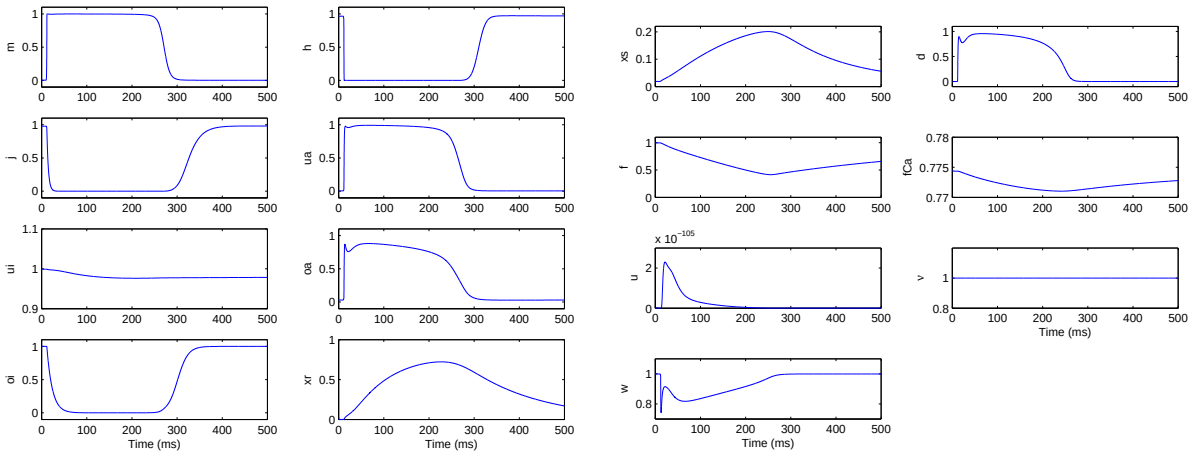

Figure 3: CRN model: gating variables.

Given $v_0, w_0, c_0 \in L^2(\Omega)$, $I^{app} \in L^2(\Omega \times (0,T))$, find $u_{i,e} \in W^{1,1}(0,T; H^1(\Omega))$, such that $\forall t \in (0,T)$

$$\begin{cases} c_m \dfrac{\partial}{\partial t}(v(t), \phi_i) + a_i(u_i(t), \phi_i) + (I_{ion}(v(t), w(t), c(t)), \phi_i) = 0 & \forall \phi_i \in H^1(\Omega) \\ -c_m \dfrac{\partial}{\partial t}(v(t), \phi_e) + a_e(u_e(t), \phi_e) - (I_{ion}(v(t), w(t), c(t)), \phi_e) = -(I_e^{app}, \phi) & \forall \phi_e \in H^1(\Omega) \\ v(\mathbf{x}, t) = u_i(\mathbf{x}, t) - u_e(\mathbf{x}, t), \end{cases} \tag{4.1}$$

coupled with the ordinary differential system (2.3), where suitable initial conditions on v, w, c are provided, as given in (2.5). In (4.1), $(.,.)$ and $a_{i,e}(.,.)$ denote the inner product in $L^2(\Omega)$

$$(\eta, \xi) = \int_\Omega \eta \xi \, dx \qquad \forall \eta, \xi \in L^2(\Omega),$$

and the elliptic bilinear forms

$$a_{i,e}(\lambda, \mu) = \int_\Omega (\nabla \lambda)^T D_{i,e}(\mathbf{x}) \nabla \mu \, dx \qquad \forall \lambda, \mu \in H^1(\Omega),$$

respectively.
The variational formulation of the monodomain model follows by replacing equations (4.1) with

$$c_m \frac{\partial}{\partial t}(v(t), \phi) + a(v(t), \phi) + (I_{ion}(v(t), w(t), c(t)), \phi) = (I^{app}, \phi) \qquad \forall \phi \in H^1(\Omega), \tag{4.2}$$

where again $(.,.)$ denotes the inner product in $L^2(\Omega)$, while $a(.,.)$ denotes the elliptic bilinear form

$$a(\lambda, \mu) = \int_\Omega (\nabla \lambda)^T D(\mathbf{x}) \nabla \mu \, dx \qquad \forall \lambda, \mu \in H^1(\Omega),$$

respectively, always coupled with the ordinary differential system (**??**).
If, on the one hand, several theoretical results on reaction-diffusion equations can be applied to the monodomain model, on the other hand less is known on degenerate reaction-diffusion systems such as the bidomain model. We refer the reader to [6] for existence, uniqueness and regularity results, both at the continuous and the semi-discrete level, and to [26] for a convergence analysis of finite elements approximations. Both papers deal with the FitzHugh-Nagumo (FHN) model of the gating system.
More results are known on the related eikonal approximation describing the propagation of excitation front (see for instance [2, 3, 12]), and a mathematical analysis of the bidomain model using Γ-convergence theory can be found in [1].

4.1 Semi-discrete formulation

Let $\mathcal{T}_h$ be a regular triangulation of $\Omega \subset \mathbb{R}^d$ $(d = 2, 3)$, namely $\Omega = \bigcup_{j=1}^{N} K_j$, where each $K_j = T_{K_j}(E) \in \mathcal{T}_h$, E is the reference element, a simplex (namely the triangle with vertices $(0, 0)$, $(1, 0)$, and $(0, 1)$ when $d = 2$ or the thetrahedron with vertices $(0, 0, 0)$, $(1, 0, 0)$, $(0, 1, 0)$, and $(0, 0, 1)$ when $d = 3$) or the unit cube $[0, 1]^d$ $(d = 2, 3)$, and where T_{K_j} is an invertible affine map. We define h as the maximum diameter of the elements of the triangulation. The associated finite element spaces X_h and Y_h (see e.g. [21] for an introduction to finite element methods) are defined as

$$X_h = \left\{ \varphi_h \in C^0(\Omega) \,|\, \varphi_{h\,|K_j} \circ T_{K_j} \in \mathbb{P}_1(E) \right\}, \qquad Y_h = \left\{ \varphi_h \in C^0(\Omega) \,|\, \varphi_{h\,|K_j} \circ T_{K_j} \in \mathbb{Q}_1(E) \right\},$$

where $\mathbb{P}_1(E)$ is the space of polynomials of degree at most one on E, whereas $\mathbb{Q}_1(E)$ is the space of polynomials of degree at most one with respect to each variable on E.
A semi-discrete problem in space is then obtained by applying a Galerkin procedure, using as finite dimensional space $V_h = X_h$ or $V_h = Y_h$, and choosing a basis for V_h. We denote by N_h the dimension of V_h, we let $\{\varphi_i\}_{i=1}^{N_h}$ be the finite element basis, and we let $M = (m_{kl})$, $A = (a_{kl})$ and $A_{i,e} = (a_{kl}^{i,e})$ be the symmetric mass and stiffnes matrices defined by

$$m_{kl} = \sum_{j=1}^{N} \int_{K_j} \varphi_k \varphi_l \, dx,$$

$$a_{kl} = \sum_{j=1}^{N} \int_{K_j} (\nabla \varphi_k)^T D(\mathbf{x}) \nabla \varphi_l \, dx \qquad a_{kl}^{i,e} = \sum_{j=1}^{N} \int_{K_j} (\nabla \varphi_k)^T D_{i,e}(\mathbf{x}) \nabla \varphi_l \, dx.$$

In the next section, devoted to numerical simulations, such integrals are evaluated by means of a 3rd order Gaussian rule.
We let

$$u_{i,h}(t, x) = \sum_{j=1}^{N_h} u_{i,j}(t)\varphi_j(x) \qquad u_{e,h}(t, x) = \sum_{j=1}^{N_h} u_{e,j}(t)\varphi_j(x) \qquad v_h(t, x) = \sum_{j=1}^{N_h} v_j(t)\varphi_j(x)$$

$$w_h(t, x) = \sum_{j=1}^{N_h} w_j(t)\varphi_j(x) \qquad c_h(t, x) = \sum_{j=1}^{N_h} c_j(t)\varphi_j(x)$$

and denoting, for sake of simplicity, by

$$\boldsymbol{u}_{i,h} = (u_{i,1}, \ldots, u_{i,N_h})^T \qquad \boldsymbol{u}_{e,h} = (u_{e,1}, \ldots, u_{e,N_h})^T \qquad \boldsymbol{v}_h = (v_1, \ldots, {}_{N_h})^T$$

$$\boldsymbol{w}_h = (w_1, \ldots, {}_{N_h})^T \qquad \boldsymbol{c}_h = (c_1, \ldots, {}_{N_h})^T$$

the bidomain formulation for the finite element problem can be written in compact form as

$$c_m \begin{bmatrix} M & -M \\ -M & M \end{bmatrix} \frac{\partial}{\partial t} \begin{bmatrix} \boldsymbol{u}_{i,h} \\ \boldsymbol{u}_{e,h} \end{bmatrix} + \begin{bmatrix} A_i & 0 \\ 0 & A_e \end{bmatrix} \begin{bmatrix} \boldsymbol{u}_{i,h} \\ \boldsymbol{u}_{e,h} \end{bmatrix} + \begin{bmatrix} M\, I_{ion}^h(\boldsymbol{v}_h, \boldsymbol{w}_h, \boldsymbol{c}_h) \\ -M\, I_{ion}^h(\boldsymbol{v}_h, \boldsymbol{w}_h, \boldsymbol{c}_h) \end{bmatrix} = \begin{bmatrix} 0 \\ M I_{e,h}^{app} \end{bmatrix}. \quad (4.3)$$

In the simpler monodomain formulation, the finite elements approximation of the transmembrane potential $\boldsymbol{v}_h$ is the solution of

$$c_m M \frac{\partial \boldsymbol{v}_h}{\partial t} + A\boldsymbol{v}_h + M\, I_{ion}^h(\boldsymbol{v}_h, \boldsymbol{w}_h, \boldsymbol{c}_h) = M I_h^{app}. \quad (4.4)$$

Both equations (4.4) and (4.3) are coupled with the semidiscrete formulation of the dynamics of the gating and concentration variables

$$\frac{\partial \boldsymbol{w}_h}{\partial t} = R(\boldsymbol{v}_h, \boldsymbol{w}_h), \qquad \frac{\partial \boldsymbol{c}_h}{\partial t} = S(\boldsymbol{v}_h, \boldsymbol{w}_h, \boldsymbol{c}_h).$$

Finally, the semi-discrete version of the alternative bidomain formulation (2.6) in terms of $\boldsymbol{v}_h$ and $\boldsymbol{u}_{e,h}$ is given by

$$\begin{cases} c_m M \dfrac{\partial \boldsymbol{v}_h}{\partial t} + A_i \boldsymbol{v}_h + A_i \boldsymbol{u}_{e,h} + M\, I_{ion}^h(\boldsymbol{v}_h, \boldsymbol{w}_h, \boldsymbol{c}_h) = M\, I_{i,h}^{app} \\ \\ A_i \boldsymbol{v}_h + (A_e + A_i)\boldsymbol{u}_{e,h} = M(I_{i,h}^{app} - I_{e,h}^{app}). \end{cases} \quad (4.5)$$

Equation (4.5) above is a Differential-Algebraic Equation (DAE), that separates the differential variable $\boldsymbol{v}_h$ from the algebraic one $\boldsymbol{u}_{e,h}$. Such approach has been firstly used in [2] and [24], and sequently by many other authors.

4.2 Fully discrete approximation

In order to have a fully discrete approximation of the problem, we integrate in time systems (4.4) and (4.3) by means of a semi-implicit Euler scheme: the linear diffusion term is discretized implicitely, while the nonlinear reaction term (the ionic current I_{ion}) is treated explicitely. The mass matrix M is lumped to diagonal form by standard techniques. Owing to the Hodgkin-Huxley formalism, the ordinary differential system for the gating variables is integrated exactly after linearization around the potential at the previous time step, and the $j-$th gating variable at time step $n+1$ is given by

$$\boldsymbol{w}_{h,j}^{n+1} = \boldsymbol{w}_{j\infty}(\boldsymbol{v}_{h,j}^{n}) + (\boldsymbol{w}_{h,j}^{n} - \boldsymbol{w}_{j\infty}(\boldsymbol{v}_{h,j}^{n}))\exp\left(-\frac{\Delta t}{\tau \boldsymbol{w}_{h,j}(\boldsymbol{v}_{h,j}^{n})}\right),$$

while the system for the concentration variables is integrated by a backward Euler scheme

$$\frac{\boldsymbol{c}_h^{n+1} - \boldsymbol{c}_h^{n}}{\Delta t} = S(\boldsymbol{v}_h^{n}, \boldsymbol{w}_h^{n+1}, \boldsymbol{c}_h^{n}).$$

This allows us to decouple the ODE system by solving with respect to the gating and concentration variables first, given the potential at the previous time step $\boldsymbol{v}_h^n$, and then solving, in the monodomain case, for $\boldsymbol{v}_h^{n+1}$

$$c_m M \frac{\boldsymbol{v}_h^{n+1} - \boldsymbol{v}_h^{n}}{\Delta t} + A\boldsymbol{v}_h^{n+1} + MI_{ion}^h(\boldsymbol{v}_h^{n}, \boldsymbol{w}_h^{n+1}, \boldsymbol{c}_h^{n+1}) = MI_h^{app}$$

and, in the bidomain case, for $\boldsymbol{u}_{i,h}^{n+1}$ and $\boldsymbol{u}_{e,h}^{n+1}$

$$\begin{cases} c_m M \dfrac{\boldsymbol{v}_h^{n+1} - \boldsymbol{v}_h^{n}}{\Delta t} + A_i \boldsymbol{u}_{i,h}^{n+1} + MI_{ion}^h(\boldsymbol{v}_h^{n}, \boldsymbol{w}_h^{n+1}, \boldsymbol{c}_h^{n+1}) = 0 \\ \\ -c_m M \dfrac{\boldsymbol{v}_h^{n+1} - \boldsymbol{v}_h^{n}}{\Delta t} + A_e \boldsymbol{u}_{e,h}^{n+1} - MI_{ion}^h(\boldsymbol{v}_h^{n}, \boldsymbol{w}_h^{n+1}, \boldsymbol{c}_h^{n+1}) = -MI_{e,h}^{app}, \end{cases}$$

where $\boldsymbol{v}_h^{n+1} = \boldsymbol{u}_{i,h}^{n+1} - \boldsymbol{u}_{e,h}^{n+1}$. With this choice (notice that one could solve for the potential first and update successively the gating and concentration variables), the semi-implicit method in the monodomain case requires to solve the linear system

$$[c_m M + \Delta t A]\, \boldsymbol{v}_h^{n+1} = c_m M \boldsymbol{v}_h^{n} - \Delta t MI_{ion}^h(\boldsymbol{v}_h^{n}, \boldsymbol{w}_h^{n+1}, \boldsymbol{c}_h^{n+1}) + \Delta t MI_h^{app},$$

while, in the bidoman case, the associated linear system is

$$\begin{bmatrix} c_m M + \Delta t A_i & -c_m M \\ -c_m M & c_m M + \Delta t A_e \end{bmatrix} \begin{bmatrix} \boldsymbol{u}_{i,h}^{n+1} \\ \boldsymbol{u}_{e,h}^{n+1} \end{bmatrix} = c_m \begin{bmatrix} M & -M \\ -M & M \end{bmatrix} \begin{bmatrix} \boldsymbol{u}_{i,h}^{n} \\ \boldsymbol{u}_{e,h}^{n} \end{bmatrix} - \Delta t \begin{bmatrix} MI_{ion}^h(\boldsymbol{v}_h^{n}, \boldsymbol{w}_h^{n+1}, \boldsymbol{c}_h^{n+1}) \\ -MI_{ion}^h(\boldsymbol{v}_h^{n}, \boldsymbol{w}_h^{n+1}, \boldsymbol{c}_h^{n+1}) - MI_{e,h}^{app} \end{bmatrix}.$$

The semi-implict scheme above leads, in the monodomain case, to a linear system with symmetric positive definite matrix, and, in the bidomain case, to a linear system with a symmetric positive semidefinite matrix, with a one dimensional kernel spanned by $(\mathbf{1}, \mathbf{1})^T$. The transmembrane potential $\boldsymbol{v}_h^{n+1}$ is then uniquely determined for both the monodomain and the bidomain models, as in the continuous model, while $\boldsymbol{u}_{i,h}^{n+1}$ and $\boldsymbol{u}_{e,h}^{n+1}$ are determined up to the same additive time-dependent constant with respect to a reference potential. Such constant can be determined by imposing the condition $\mathbf{1}^T M \boldsymbol{u}_{e,h}^{n+1} = 0$. Both systems are solved by a preconditioned conjugate gradient algorithm (PCG), using as initial guess the solution at the previous time step.

5 Numerical simulations

In this section we describe some numerical simulations. We consider two dimensional domains since the thickness of the atrial wall is far less significant than that of the ventricular one, and a two dimensional approximation is thus reasonable. We run monodomain and bidomain simulations, with both the modified FHN and the CRN cell model. In Table 1 we report the parameter calibration for the tests. The numerical simulations are run on MATLAB® 6.5.

General	$\chi = 10^3\ cm^{-1}$	$C_m = 10^{-3}\ mF/cm^2$
Monodomain	$\sigma_l = 1.2 \cdot 10^{-3}\ \Omega^{-1}cm^{-1}$	$\sigma_t = 2.5562 \cdot 10^{-4}\ \Omega^{-1}cm^{-1}$
Bidomain	$\sigma_l^e = 2 \cdot 10^{-3}\ \Omega^{-1}cm^{-1}$	$\sigma_t^e = 1.3514 \cdot 10^{-4}\ \Omega^{-1}cm^{-1}$
	$\sigma_l^i = 3 \cdot 10^{-3}\ \Omega^{-1}cm^{-1}$	$\sigma_t^i = 3.1525 \cdot 10^{-4}\ \Omega^{-1}cm^{-1}$
FHN model	$G = 1.5\ \Omega^{-1}cm^{-2}$	$\eta_1 = 4.4\Omega^{-1}cm^{-1}$
	$v_{th} = 13\ mV$	$\eta_2 = 0.012$
	$v_p = 100\ mV$	$\eta_3 = 1$
CRN model	As in the original paper [7]	

Table 2: Parameter calibration for the numerical simulations

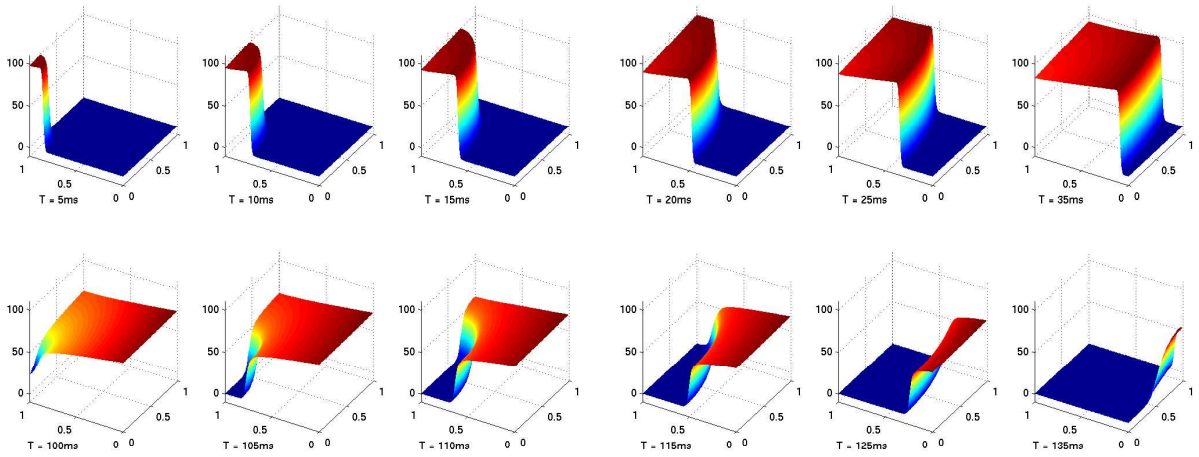

Figure 4: Monodomain FHN on a 2d slab: excitation and repolarization

5.1 Numerical simulation of a slab

In this first series of tests the computational domain is $\Omega = [0,1] \times [0,1]$, and the problem is discretized by $\mathbb{P}_1$ elements on an unstructured triangular grid. In the first test we considered a vertex stimulation of the slab. We show the spread of excitation and the repolarization, in Figure 4 for the monodomain-FHN model, and, in Figure 5 for the monodomain-CRN model. For the latter model, the spike-and-dome profile of the Action Potential is more evident, as well as the longer time needed to recover the resting value of the potential, owing to the presence of the plateau phase, that is not captured by the simple FHN model.

In the second test we considered a central stimualtion of the slab. We show the transmembrane potential v as well as the intracellular and extracellular potentials u_i and u_e, in figure 6 for the bidomain FHN model, at point (.2333,.5667) of the slab, in figure 7 for the bidomain CRN model at point (.8,.7).

In the third test, in order to simulate the presence of arteries or veins, we considered a two dimensional

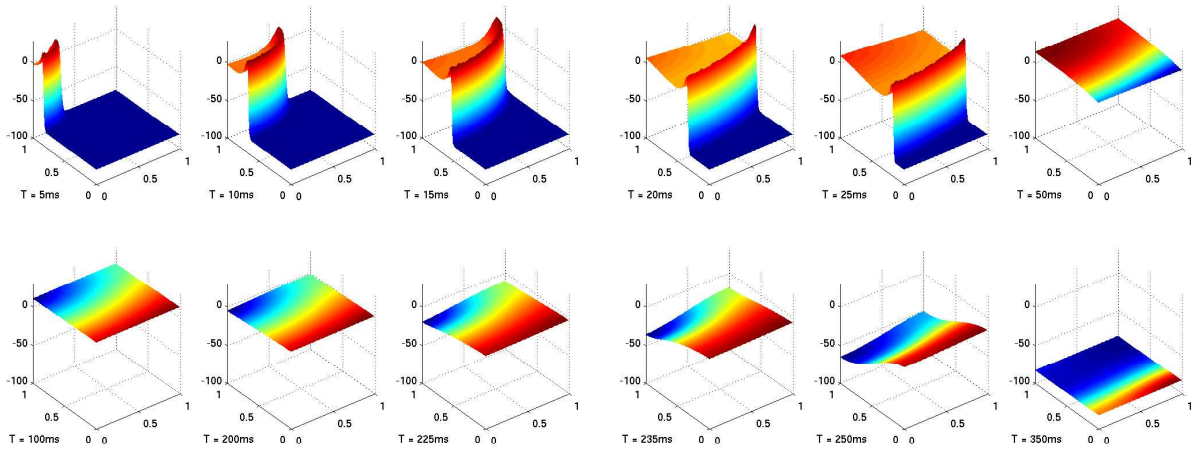

Figure 5: Monodomain CRN on a 2d slab: excitation and repolarization

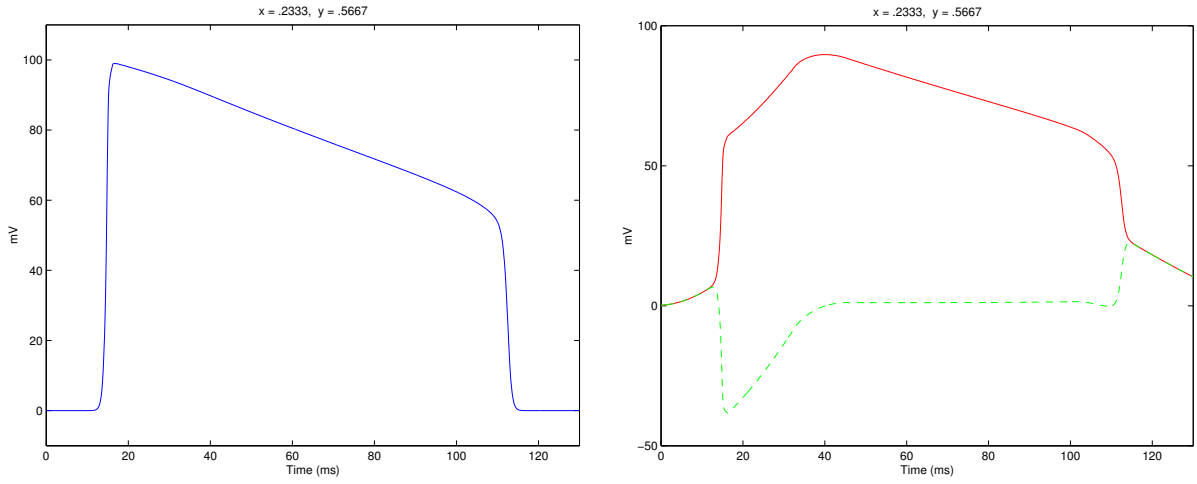

Figure 6: Bidomain FHN on a 2d slab: transmembrane potential v (left), intracellular u_i (solid line) and extracellular u_e (dotted line) potential at point (.2333,.5667)

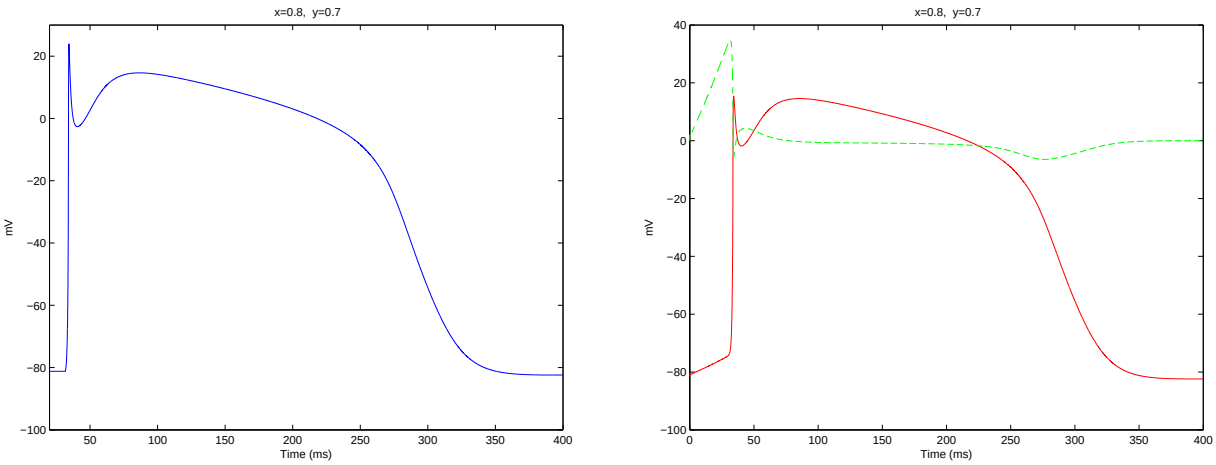

Figure 7: Bidomain CRN on a 2d slab: transmembrane potential v (left), intracellular u_i (solid line) and extracellular u_e (dotted line, magnified by a factor 5) potential at point (0.8,0.7)

slab with a circular hole embedded. Since the vessel walls (both arterious and venous) are not excitable, we impose a non-conducting condition ($\boldsymbol{n} \cdot \nabla \boldsymbol{v} = 0$) on the border of the hole. We show the spread of excitation and the repolarization for the monodomain FHN model in Figure 8, and for the monodomain CRN in Figure 9. In Figure 10, a closer look allows to better appreciate the distorsion of the wavefront in the neighbourhood of the hole for both the FHN and CRN bidomain models.

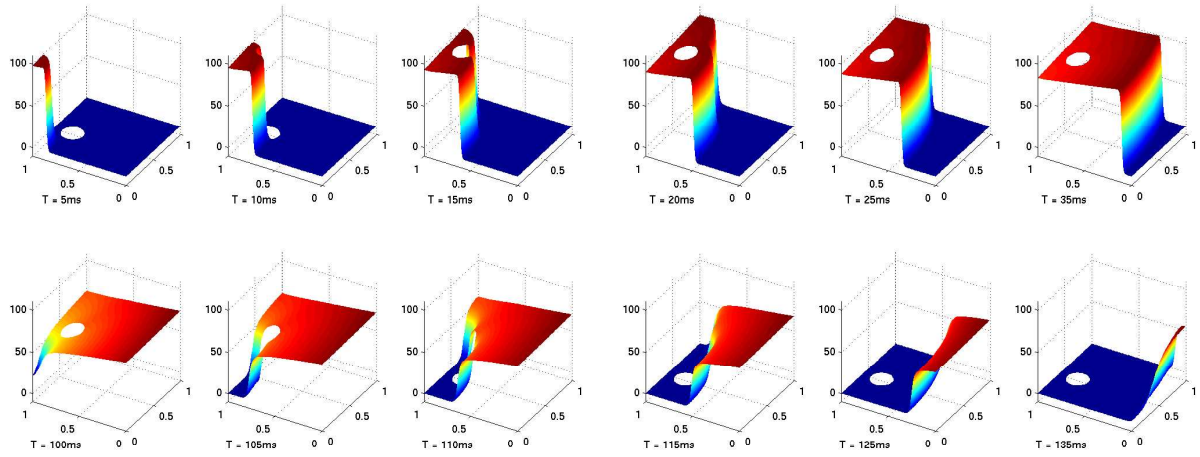

Figure 8: Monodomain FHN on a 2d slab with an hole: excitation and repolarization

5.2 Numerical simulation on curved surfaces

In this second series of tests we consider curved surfaces. In the first test we consider the unit sphere as a coarse model of the atrium and we run bidomain simulation for both the FHN and the CRN cell models. We plot in figure 11 and 12 the spread of excitation on the sphere for the two models.

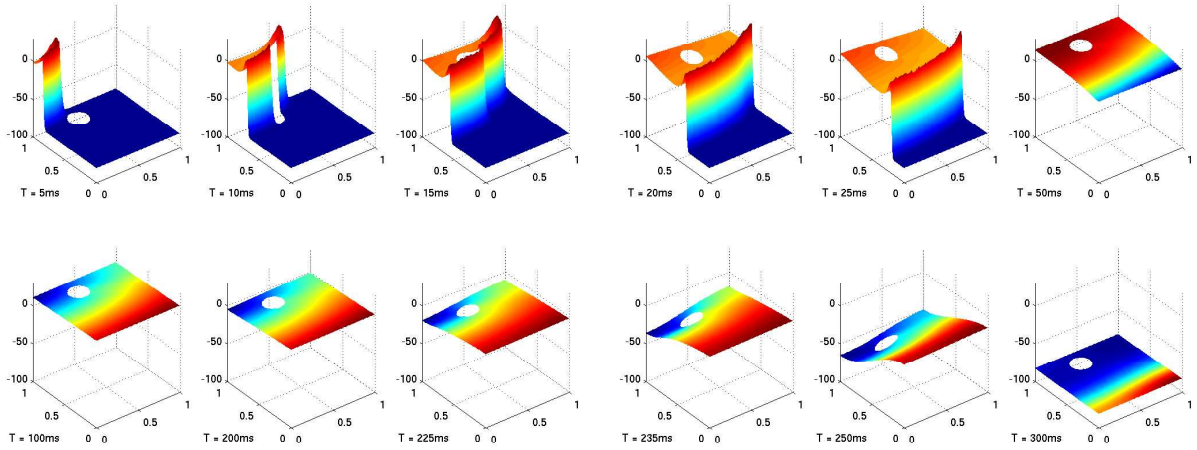

Figure 9: Monodomain CRN on a 2d slab with an hole: excitation and repolarization

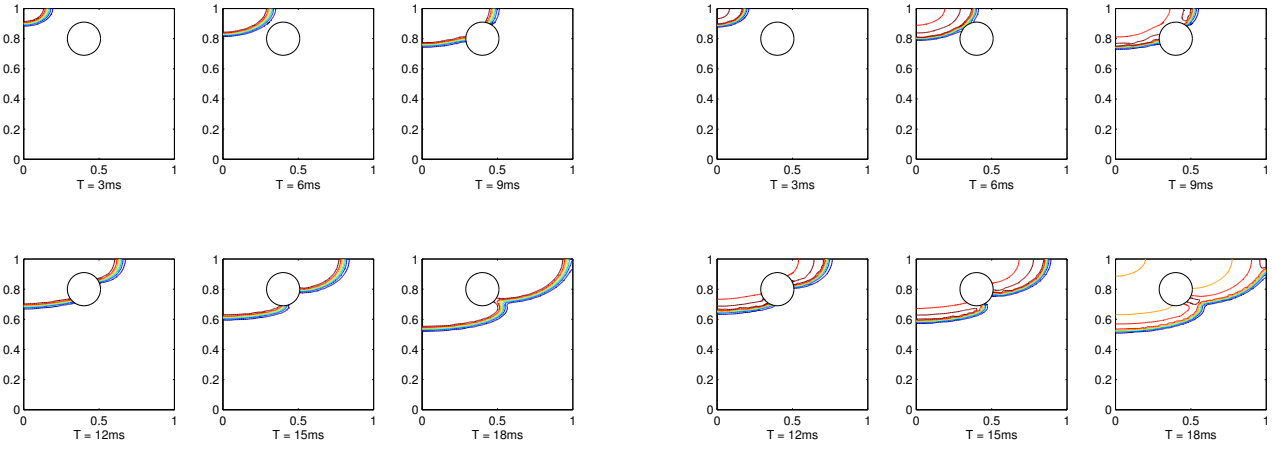

Figure 10: Propagation wavefront aroud an hole: bidomain FHN (left) and CRN (right) models

In the second test we consider a coarse approximate geometrical model of both atria. The stimulus is located in a position corresponding to the one of the sinus node and we run an entire heartbeat. We plot in figures 13 and 14 the spread of excitation along these atrial chambers.

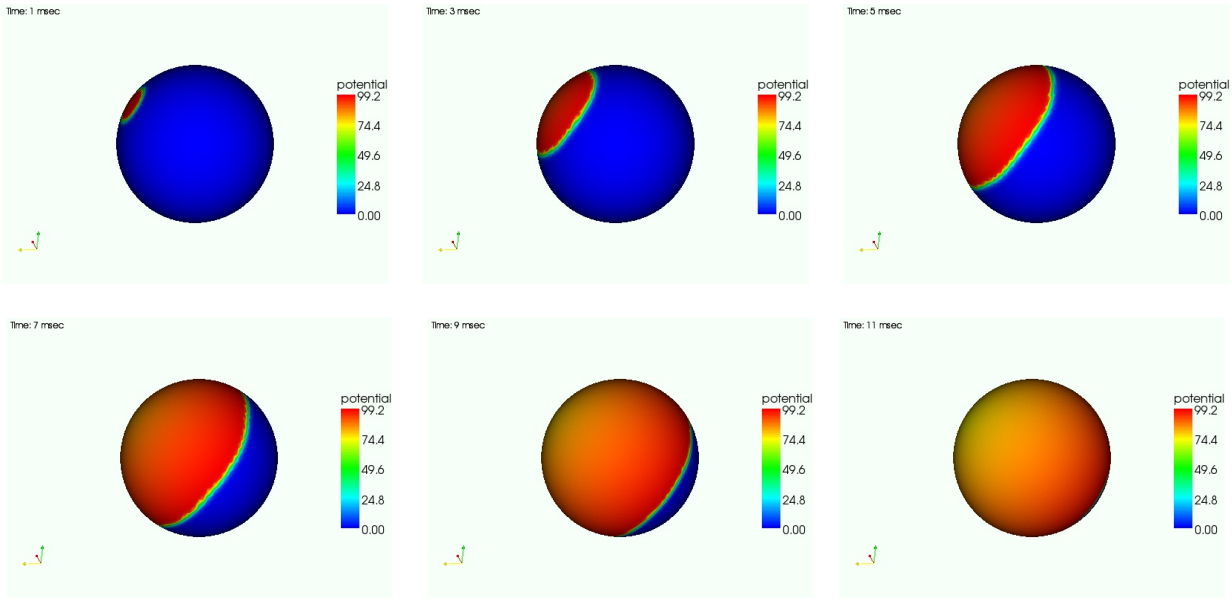

Figure 11: Propagation wavefront on a sphere: bidomain FHN model

6 Conclusions

We presented here an approach to simulate the propagation of the excitation fronts in the atrial cells, based on nonlinear models of reaction-diffusion type, considering both the monodomain and the bidomain approach. The ionic currents are expressed by the simple modified FHN model (in the Rogers-McCulloch variant), and by the more sophisticated CRN model, especially designed for human atrial cells. Numerical simulations on a two dimensional slab, on a sphere, and on a coarse model of the atria are given to show the behaviour of the excitation spread and the repolarization phase. The extension of such simulations to a more realistic geometry is currently under investigation. Further directions of research will be twofold: on the one hand we will include in the model the presence of pacemaker cells as the ones provided by O. Doessel and his collaborators (see for instance [27] and [28]), and on the other hand we will couple the atrial simulation with the ventricular one by embedding in the framework the cell model for atrioventricular node proposed by L. Glass and his collaborators [11].

References

[1] L. Ambrosio, P. Colli Franzone, and G. Savaré. On the asymptotic behaviour of anisotropic energies arising in the cardiac bidomain model. *Interfaces Free Bound.*, 2:213–266, 2000.

[2] P. Colli Franzone and L. Guerri. Spread of excitation in 3-D models of the anisotropic cardiac tissue, I: Validation of the eikonal approach. *Math. Biosci.*, 113:145–209, 1993.

[3] P. Colli Franzone, L. Guerri, M. Pennacchio, and B. Taccardi. Spread of excitation in 3-D models of the anisotropic cardiac tissue, II: Effect of the fiber architecture and ventricular geometry. *Math. Biosci.*, 147:131–171, 1998.

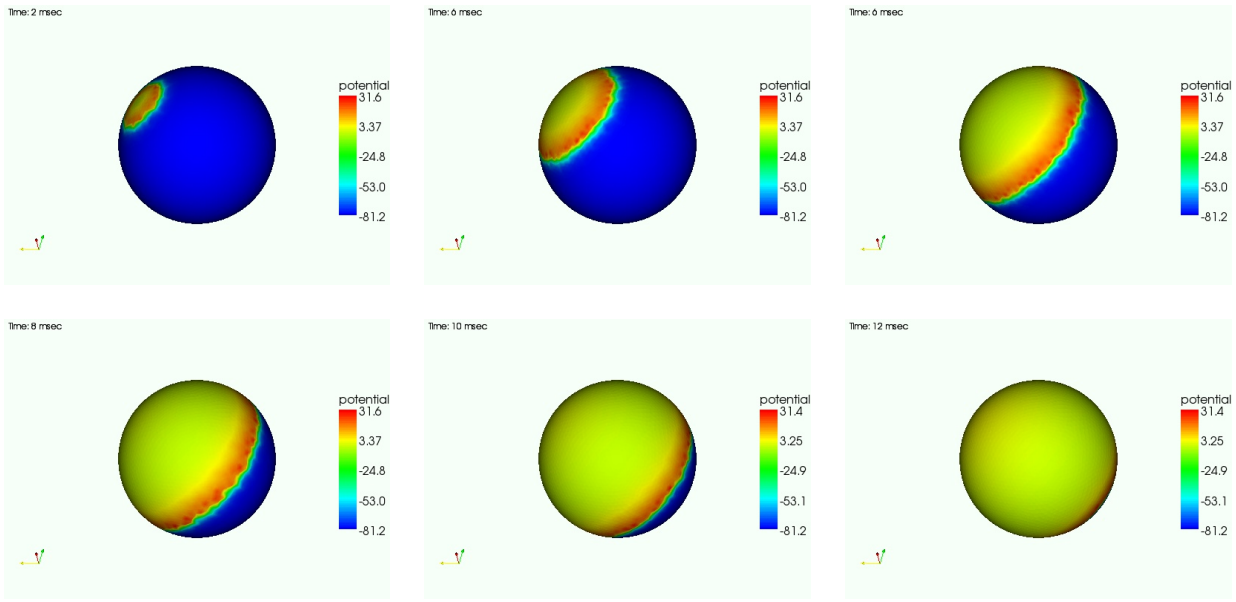

Figure 12: Propagation wavefront on a sphere: bidomain CRN model

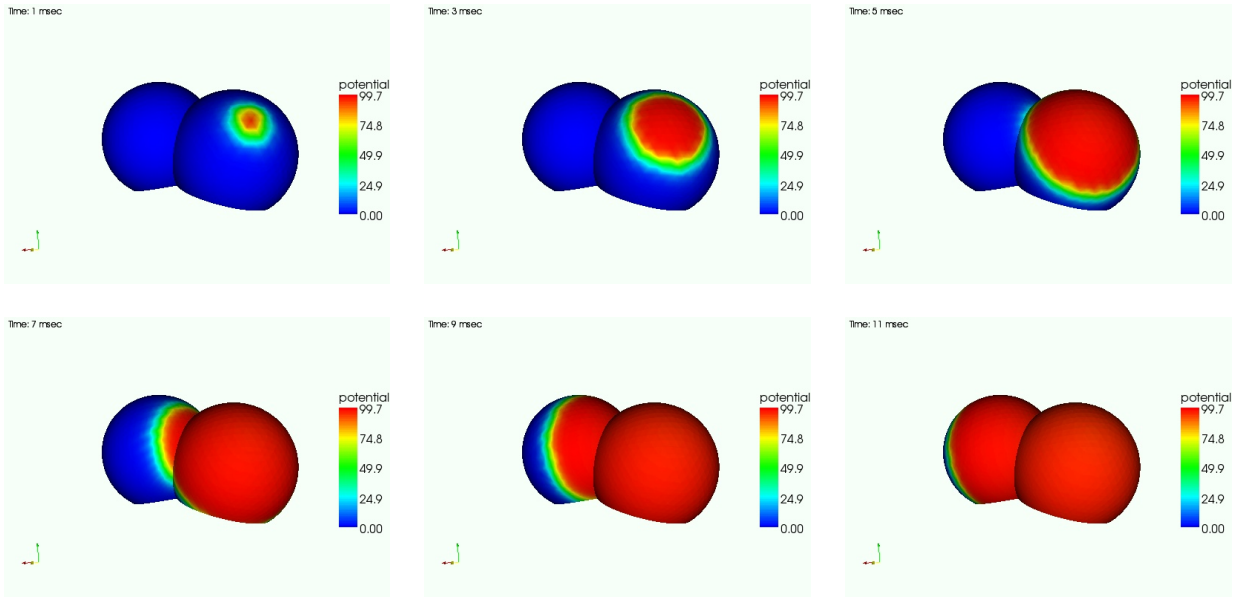

Figure 13: Propagation wavefront on atrial chambers: bidomain FHN model

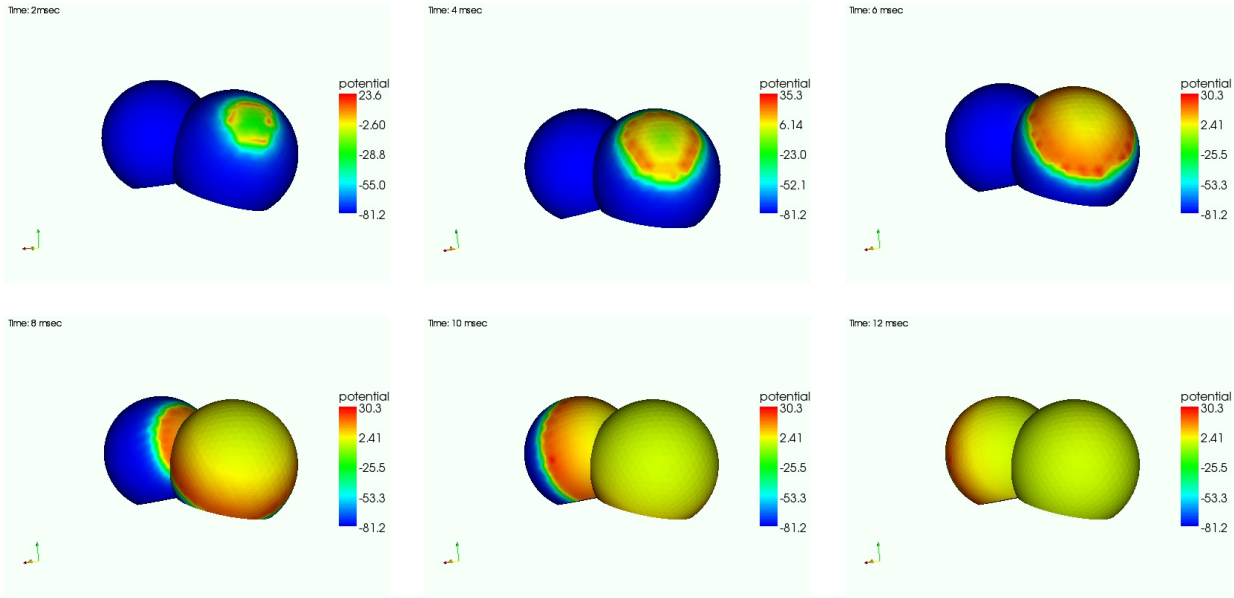

Figure 14: Propagation wavefront on atrial chambers: bidomain CRN model

[4] P. Colli Franzone and L.F. Pavarino. A parallel solver for reaction-diffusion systems in computational electrocardiology. *Mathy. Mod. Meth. Appl. Sci.*, 14(6):883–911, 2004.

[5] P. Colli Franzone, L.F. Pavarino, and B. Taccardi. Simulating patterns of excitation, repolarization and action potential duration with cardiac Bidomain and Monodomain models. *Math. Biosci.*, 197(1):35–66, 2005.

[6] P. Colli Franzone and G. Savaré. Degenerate evolution systems modeling the cardiac electric field at micro and macroscopic level. In A. Lorenzi and B. Ruf, editors, *Evolution Equations, Semigroups and Functional Analysis*, pages 49–78. Birkhauser, 2002.

[7] M. Courtemanche, R.J. Ramirez, and S. Nattel. Ionic mechanisms underlying human atrial action potential properties: insights from a mathematical model. *Am. J. Physiol.*, 275 (Heart Circ. Physiol. 44):H301–H321, 1998.

[8] Y.E. Earm and D. Noble. A model of the single atrial cell: relation between calcium current and calcium release. *Pro. R. Soc. London B Biol. Sci.*, 240:83–96, 1990.

[9] C.S. Henriquez. Simulating the electrical behavior of cardiac tissue using the bidomain model. *Crit. Rev. Biomed. Engrg.*, 21:1–77, 1993.

[10] A.L. Hodgkin and A.F. Huxley. A quantitative description of membrane current and its application to conduction and excitation in nerve. *J. Physiol.*, 117:500–544, 1952.

[11] P. Jørgensen, C. Schäfer, P.G. Guerra, M. Talajic, S. Nattel, and L. Glass. A mathematical model of human atrioventricular nodal function incorporating concealed conduction. *Bulletin of Mathematical Biology*, 64(6):1083–1099, 2002.

[12] J.P. Keener. An eikonal-curvature equation for the action potential propagation in myocardium. *J. Math. Biol.*, 29:629–651, 1991.

[13] J.P. Keener and J. Sneyd. *Mathematical Physiology*. Springer-Verlag, 1998.

[14] J. Kneller, R. Zou, E.J. Vigmond, Z. Wang, L.J. Leon, and S. Nattel. Cholinergic atrial fibrillation in a computer model of a two-dimensional sheet of canine atrial cells with realistic ionic properties. *Circ. Res.*, 90:e73–e87, 2002.

[15] J. Le Grice, B.H. Smaill, L.Z. Chai, S.G. Edgar, J.B. Gavin, and P.J. Hunter. Laminar structure of the heart: ventricular myocyte arrangement and connective tissue architecture in the dog. *Am. J. Physiol.*, 269 (Heart Circ. Physiol.):H571–H582, 1995.

[16] D.S. Lindblad, C.R. Murphey, J.W. Clark, and W.R. Giles. A model of the action potential and underlying membrane currents in a rabbit atrial cell. *Am. J. Physiol.*, 271:H1666–H1696, 1996.

[17] C. Luo and Y. Rudy. A dynamic model of the cardiac ventricular action potential. *Circ. Res.*, 74:1071–1096, 1994.

[18] A. Nygren, C. Fiset, L.Firek, J.W. Clark, D.S. Lindblad, R.B. Clark, and W.R. Giles. Mathematical model of an adult human atrial cell: the role of K+ currents in repolarization. *Circ. Res.*, 82:63–81, 1998.

[19] A.V. Panfilov. Spiral breakup as a model of ventricular fibrillation. *Chaos*, 8:57–64, 1998.

[20] A.V. Panfilov and A.V. Holden. *Computational biology of the heart*. Wiley, 1997.

[21] A. Quarteroni and A. Valli. *Numerical Approximation of Partial Differential Equations*. Springer-Verlag, Berlin, 1994.

[22] R.L. Rasmusson, J.W. Clark, W.R. Giles, E.F. Shibata, and D.L. Campbell. A mathematical model of a bullfrog cardiac pacemaker cell. *Am. J. Physiol.*, 259:H352–H369, 1990.

[23] J.M. Rogers and A.D. McCulloch. A collocation-galerkin finite element model of cardiac action potential propagation. *IEEE Trans. Biomed. Engnrg.*, 41:743–757, 1994.

[24] B.J. Roth. Action potential propagation in a thick strand of cardiac muscle. *Circ. Res.*, 68:162–173, 1991.

[25] B.J. Roth. How the anisotropy of the intracellular and extracellular conductivity influence stimulation of cardiac muscle. *J. Mat. Biol.*, 30:633–646, 1992.

[26] S. Sanfelici. Convergence of the galerkin approximation of a degenerate evolution problem in electrocardiology. *Numer. Meth. Part. Diff. Eq.*, 18(2):218–240, 2002.

[27] G. Seemann. *Modeling of Electrophysiology and tension development in the human heart*. PhD thesis, Universität Karlsruhe, 2005.

[28] G. Seemann, C. Höper, F.B. Sachse, O. Dössel, A.V. Holden, and H. Zhang. Heterogeneous three-dimensional anatomical and electrophysiological model of human atria. *Phil. Trans. Royal Society A*, 364(1843):1465–1481, 2006.

[29] D. Streeter. Gross morphology and fiber geometry in the heart. In R.M. Berne, editor, *Handbook of Physiology*, volume 1 (Sec. 2), pages 61–112. Williams and Wilnkins, 1979.

[30] K.H.W.J. Ten Tusscher and A.V. Panfilov. Wave propagation in excitable media with randomly distributed obstacles. *Multiscale Model. Simul.*, 3(2):265–282, 2005.

[31] R.L. Winslow, A. Varghese, D. Noble, C. Adlakha, and A. Hoythya. Generation and propagation of ectopic beats induced by spatially localized Na-K pump inhibition in atrial network models. *Pro. R. Soc. London B Biol. Sci.*, 254:55–61, 1993.

[32] H. Zhang, A.V. Holden, I. Kodama, H. Honjo, M. Lei, T. Varghese, and M.R Boyett. Mathematical models of action potentials in the periphery and center of the rabbit sinoatrial node. *Am. J. Physiol.*, 279 (Heart Circ. Physiol.):H397–H421, 2000.